Journal of Vertebrate Paleontology e2498453 (14 pages)

DOI: 10.1080/02724634.2025.2498453

ARTICLE

A NEW PREDATORY ACTINOPTERYGIAN FROM THE TOURNAISIAN OF NOVA SCOTIA PROVIDES INSIGHT INTO THE EVOLUTION OF ACTINOPTERYGIAN FEEDING

CONRAD D. WILSON, *[,1] CHRIS F. MANSKY,[2] and JASON S. ANDERSON [3]
[1]Department of Earth Sciences, Carleton University, Ottawa, Ontario, K1S 5B6, Canada, conraddwilson@gmail.com;
[2]Blue Beach Fossil Museum, Hantsport, Nova Scotia, B0P 1P0, Canada, bbfossils2023@gmail.com;
[3]Comparative Biology and Experimental Medicine, Faculty of Veterinary Medicine, University of Calgary, Calgary, Alberta, K1Y 4N1, Canada, janders@ucalgary.ca

ABSTRACT—The Devonian–Carboniferous transition represents a fundamental shift in vertebrate faunal composition and ocean ecology. Tournaisian-aged outcrops of the Horton Bluff Formation from Blue Beach, Nova Scotia capture this moment and yield a diverse fauna of actinopterygians and other vertebrates. Here, we report an actinopterygian mandible preserved in 3D, representing a new genus and species, *Sphyragnathus tyche*. This mandible is elongate, deeply curved, and bears a primary dentition of heterodont fangs. Actinopterygian identity is established by the characteristic ornamentation, dentition, and overall mandible construction observed in the specimen. Analysis of the relationship between mandible and body length in Paleozoic actinopterygians establishes *S. tyche* as a relatively large actinopterygian. Mandible length, curvature, and fang morphology combine to produce a functionally differentiated dentition with distinct regions for prey capture and prey processing. Comparison with modern actinopterygians places *S. tyche* as a back-fanged macrodont, distinguishing it from front-fanged macrodont actinopterygians of the Late Devonian. This earliest known instance of back-fanged macrodonty in the actinopterygian fossil record provides further evidence of actinopterygian morphological differentiation post-Devonian and implies experimentation in feeding mode. Apparent changes in feeding mode are underscored by analysis of stress distribution across the dentition of Devonian front-fanged macrodont actinopterygians and *S. tyche*. Although this specimen is compatible with a previous 'head-first' model of morphological diversification in early Carboniferous actinopterygians, we argue that a 'feeding-first' model is a better fit.

http://zoobank.org/LSID_to_be_updated_with_proofs

SUPPLEMENTARY FILES—Supplementary files are available for this article for free at www.tandfonline.com/UJVP

Citation for this article: Wilson, C. D., Mansky, C. F., & Anderson, J. S. (2025) A new predatory actinopterygian from the Tournaisian of Nova Scotia provides insight into the evolution of actinopterygian feeding. *Journal of Vertebrate Paleontology*. https://doi.org/10.1080/02724634.2025.2498453

Submitted: October 15, 2024
Revisions received April 14, 2025
Accepted: April 15, 2025

INTRODUCTION

Our understanding of early actinopterygian evolution is in flux. A direct reading of the fossil record suggests that actinopterygians underwent a diversification during the early Carboniferous: Devonian actinopterygians are known from a handful of lineages within broadly similar bodyplans, but Carboniferous actinopterygians are diverse and morphologically disparate (Friedman & Sallan, 2012; Henderson et al., 2022). This diversification has been hypothesized as the consequence of a mass extinction (termed the Hangenberg) at the end of the Devonian that selectively affected vertebrates (Sallan & Coates, 2010), but a specific model of change—extinction recovery, adaptive radiation, or ecological release—has never been tested (Henderson et al., 2022). Furthermore, an incomplete fossil record, significant geographic bias, phylogenetic uncertainty exacerbated by prevalent "wastebasket" genera subsuming diverse actinopterygians, and taphonomic bias raise the possibility that a direct reading of the fossil record might be misleading and highly sensitive to new data (Giles et al., 2017; Henderson et al., 2022).

Indeed, recent studies have significantly altered interpretations of Hangenberg extinction selectivity for actinopterygians, both in terms of morphology and phylogeny. A putative decrease in actinopterygian mean body size driven by the Hangenberg extinction (i.e., a Lilliput effect) (Sallan & Galimberti, 2015) was not replicated by Giles et al. (2023). Instead, Giles et al. (2023) found that Hangenberg-surviving actinopterygians were generally mid-sized and that Devonian-Carboniferous actinopterygians more broadly experienced a gradual mean body-size decrease without any sharp change linked to the Hangenberg extinction. As for phylogeny, the inclusion of newly described Late Devonian (Giles et al., 2023) and Carboniferous taxa (Wilson et al., 2018) in phylogenetic analyses has produced topologies suggesting a more inclusive actinopterygian survivorship than previously indicated. Although the instability of early actinopterygian phylogenies means these results should be treated with caution (Giles et al., 2017), the best interpretation of the current data suggests that a cryptic diversification of Devonian actinopterygians produced multiple mid-sized Hangenberg-

*Corresponding author.
Color versions of one or more of the figures in the article can be found online at www.tandfonline.com/ujvp.

surviving lineages (Giles et al., 2023), which underwent more conspicuous morphological and functional diversification in the Carboniferous (Henderson et al., 2022; Sallan & Friedman, 2012).

The morphological and functional diversification of Devonian–Carboniferous actinoptergyians was analyzed by Sallan and Friedman (2012) under an explicit mass-extinction framework. This analysis used a two-dimensional morphospace to examine the pattern of morphological change in the early Carboniferous actinopterygian and post-Cretaceous acanthopterygian radiations as a test of the 'general vertebrate model' (Sallan & Friedman, 2012). The 'general vertebrate model' proposes that trait divergences during adaptive radiations proceed in a predictable sequence: first in traits related to locomotion and associated with habitat preference, then in feeding-related cranial morphology, and finally in traits under sexual selection (Friedman & Sallan, 2012; Streelman & Danley, 2003). Sallan and Friedman (2012) found that actinopterygian cranial disparity increased before actinopterygian post-cranial disparity in both cases, so Sallan and Friedman (2012) hypothesized a head/feeding-first (and trunk/locomotion-second) model of morphological diversification for actinopterygians, contradicting the general vertebrate model.

However, subsequent research has challenged the head-first/feeding-first model in early Carboniferous actinopterygians by revealing cryptic and/or unexpected morphological diversification. A re-examination of *Trawdenia planti* with μCT scanning found that the three-dimensional structure of its pectoral fin was adapted for rowing and not lift-generation—a first for actinopterygians (Coates & Tietjen, 2018). Furthermore, the absence of lift-generation in the pectoral fin of *T. planti* implies the presence of a swim bladder to counteract the overall negative buoyancy of the animal (Coates & Tietjen, 2018). Thus, *T. planti* demonstrates significant post-cranial morphological disparity related to changes in locomotory mode undetectable by two-dimensional analysis of ecomorphological traits. This is a challenge for the head-first/feeding-first hypothesis because 1) the hypothesis depends on a two-dimensional analysis of ecomorphological traits that cannot detect the functionally relevant morphological changes displayed by this specimen and 2) the hypothesis predicts that post-cranial morphological diversity should be limited and the new locomotory implied by the specimen should not be present. Despite lacking a head, the description of a 'platysomid' deep-bodied actinopterygian from the Tournaisian of Nova Scotia also weakened the head-first hypothesis (Wilson et al., 2021). This specimen demonstrated a new actinopterygian bodyplan related to a new locomotory mode and increased the postcranial morphological disparity known for earliest Carboniferous actinopterygians; this contradicts the prediction of the head-first hypothesis that, whatever the status of the specimen's head, this post-cranial disparity and new locomotory mode should not be present.

The feeding-first hypothesis remains viable despite these challenges to the head-first hypothesis because the two hypotheses are overlapping but not equivalent. Sallan and Friedman (2012) preferred a model where new cranial morphologies were adaptations for feeding, but a scenario in which early morphological adaptations for feeding also appeared in the postcranium is also possible. Feeding in fish is generally integrated with locomotion (Collar et al., 2008; Rice & Hale, 2010). Jaw movement in fish recruits the pectoral girdle (Lauder, 1980; Schaeffer & Rosen, 1961). Axial musculature has a critical role in suction-feeding strikes as well (Camp et al., 2020), with more than 90% contraction of axial muscles reported in strikes of a diverse sample of suction-feeding fish (Li et al., 2022). Furthermore, body shape and locomotory mode have a strong influence on feeding strike (e.g., Lemberg et al., 2019; Perevolotsky et al., 2020). A head-first, but not feeding-first, model is also logically possible (if less biologically likely) since the head of fishes must also be adapted for hydrodynamic (Fletcher et al., 2014), respiratory, and sensory roles (Gans & Northcutt, 1983). A neutral version of the feeding-first hypothesis would predict changes in both cranial and post-cranial morphology in the absence of any auxiliary hypotheses.

Based on the hypothesis that early Carboniferous morphological diversification in actinopterygians is related to adaptation for feeding (i.e., the neutral version of the feeding-first hypothesis), we predict that Carboniferous actinopterygians should have diverse morphologies related to feeding, including new morphologies not seen in Devonian actinopterygians. At a functional level, these new morphologies should augment new feeding strategies, leading to differences in how feeding-related morphologies are used and differences in feeding-related success. Here, we describe a new genus and species of actinopterygian with an elongated jaw bearing large fangs—characteristic predatory adaptations in actinopterygians (Barnett et al., 2006; Wainwright and Bellwood, 2002)—from the Tournaisian stage of Blue Beach, Nova Scotia (Fig. 1). First, we estimated the total and standard lengths of this new taxon to establish its context in actinopterygian body size evolution. Then, we compared this new taxon to Devonian actinopterygians with elongate, large-fanged jaws (i.e., macrodonts; *Austelliscus ferox* [Figueroa et al., 2021]) and *Tegeolepis clarki* (Dunkle & Schaeffer, 1973), on an ecomorphological and functional basis as a preliminary test of the feeding-first hypothesis. To do so, we placed these taxa into ecomorphological categories related to feeding behavior (Mihalitsis & Bellwood, 2019) and calculated the theoretical distribution of stress (Cohen et al., 2020a, 2020b). Under the feeding-first hypothesis, we predicted that this new Carboniferous taxon should belong to a different ecomorphological category and have a different theoretical stress distribution compared to Devonian taxa with elongate jaws and large fangs (i.e., *Austelliscus ferox* (Figueroa et al., 2021) and *Tegeolepis clarki* (Dunkle & Schaeffer, 1973). The absence of post-cranial material in the specimens analyzed means that our test of the head-first and feeding-first hypotheses is incomplete because the relative timing of cranial/post-cranial morphological diversification cannot be established. Nevertheless, this test is still useful because the head-first and feeding-first hypotheses generate predictions that have an opportunity to fail if we do not observe differences in mandibular morphology, ecomorphological categorization, or theoretical stress distribution between the Devonian and Carboniferous actinopterygians examined.

GEOLOGIC SETTING

The outcrops at the Blue Beach locality are part of the Horton Bluff Formation, which is wedged unconformably between rocks of the underlying Ordovician–Devonian Meguma Group and the overlying late Tournaisian Cheverie Formation (Martel et al., 1993). The geology of the Horton Bluff Formation (HBF) has been studied intensively for more than a century (see Mansky and Lucas [2013] for a complete bibliography). The HBF is subdivided into four Members—Harding Brook, Curry Brook, Blue Beach, and Hurd Creek—which span the Late Devonian and early Carboniferous in ascending order (Martel et al., 1993; Martel & Gibling, 1996; Tang et al., 2024). Only the Blue Beach and Hurd Creek Members crop out at the Blue Beach locality, where they have been dated to the middle to late Tournaisian (Tn2–Tn3) (Martel et al., 1993) (Fig. 1). These strata bear substantial structural evidence of landslides as well as soft-sediment and tectonic deformation, but are highly fossiliferous, preserving diverse plants, invertebrates, fishes, and tetrapods (Tang et al., 2024). These fossils are usually found among intertidal debris along the western bank of the Avon River (Anderson et al., 2015; Mansky & Lucas, 2013).

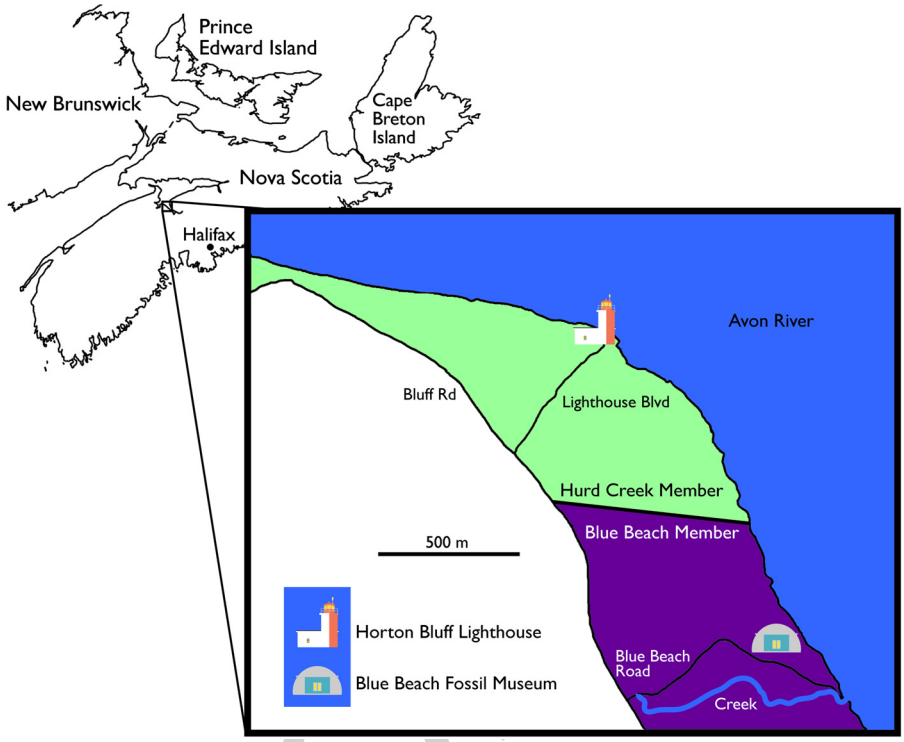

FIGURE 1. Map showing the geographic and geologic context of the Blue Beach locality modified from Anderson et al. (2015). Purple, Blue Beach Member of the HBF; green, Hurd Creek Member of the HBF.

The Blue Beach Member has been divided into between four and seven primary lithofacies, with varying numbers of subfacies (Mansky & Lucas, 2013; Martel & Gibling, 1991; Tang et al., 2024). Most recently, Tang et al. (2024) recognized seven primary lithofacies: black shale, planar siltstone, carbonate, turbidite sandstone and siltstone, wave-ripple sandstone and siltstone, channel sandstone, and hummocky cross-stratified sandstone and siltstone. These are organized into repeated cycles, which make up a generally coarsening-up and shallowing-up sequence (Martel & Gibling, 1991; Tang et al., 2024). Tang et al. (2024) established two environmental stages for the Blue Beach Member comprising 1) an offshore, deepwater environment fluctuating below wave base, and 2) a stage covering the transition from deepwater to nearshore, wave-dominated environments.

The salinity of the Blue Beach paleoenvironment has been controversial. Martel and Gibling (1991) originally interpreted the paleoenvironment as a large freshwater lake. Subsequently, Tibert and Scott (1999) reinterpreted it as a lagoonal, marginal marine environment based on the presence of marine invertebrates. Martel and Gibling (1996) revised their interpretation to include occasional connection of the paleolake to the ocean. Most recently, Tang et al. (2024) followed this interpretation and suggested that marine influence was initially intermittent and later declined.

METHODS

Imaging Methods

JSA photographed NSM 005.GF.045.260 using a Nikon D200 DSLR and a standard optical lens. CDW photographed remaining specimens using a Sony a5000 mirrorless camera and standard optical and macro lenses. CDW scanned NSM 005.GF.045.260 in the McCaig Institute for Bone and Joint Health, University of Calgary, Calgary, Alberta using a SkyScan 1173 at 130 kV and 61 µA and with a resolution of 69.58 µm. As this specimen was large, it was scanned twice, iteratively, using the oversize setting and reconstructed accordingly. Reconstruction was performed in nRecon 1.6.6.0. We cropped the resulting images in ImageJ to produce an image stack (Supplementary File 1) that was imported into Amira 4.4.0 for segmenting. The specimen was downsampled by a factor of three in the z-axis during the data import phase (for an initial voxel size of 69.58 × 69.58 × 208.75 µm). We then averaged the data by a factor of two in the other axes during the surface generation phase, resulting in a 139.16 × 139.16 × 208.75 µm voxel size for generating the final model (Supplementary File 2).

Size Estimation

We first estimated the total length of *Austelliscus ferox*, and *Tegeolepis clarki*, and the new actinopterygian taxon using the method and data of Figueroa et al. (2021). This method estimates total length by multiplying mandible length by the range of ratios between total length and mandible lengths obtained from lateral view reconstructions of eight Paleozoic actinopterygians (Supplementary File 3). We measured the mandible length of NSM.005.GF.045.260 using the measure function in Amira 4.4.0 and took mandible lengths for *Austelliscus ferox* (Figueroa et al., 2021), *Howqualepis rostridens* (Long, 1988), and *Tegeolepis clarki* (Dunkle & Schaeffer, 1973) from the literature.

We replicated the linear regression performed by Giles et al. (2023) between the natural logarithms of mandible and standard length for 55 specimens covering 20 Paleozoic actinopterygian taxa. We did an additional linear regression between raw mandible and standard lengths for the same specimens and taxa. We did both linear regressions in Microsoft Excel Version 2404 Build 16.0.17531.20140 using the Regression function from the Analysis ToolPak add-in (Supplementary File 3). However, we only used the raw length data as the basis for length estimations reported here. The correlation between mandible length and standard length was slightly lower for the raw data ($r = 0.93$) than for the logarithmically transformed data ($r = 0.95$; Supplementary File 3) but allowed a more intuitive calculation and

representation of the 95% confidence interval. Thus, we estimated the standard length of NSM 005.GF.045.260, *Austelliscus ferox*, *Howqualepis rostridens*, and *Tegeolepis clarki* from the raw length data of Giles et al. (2023) using the Forecast.Linear function and calculated 95% prediction intervals from the underlying parameters in Excel (Supplementary File 3).

Ecomorphological Categorization

We assigned NSM 005.GF.045.260, *Austelliscus ferox*, and *Tegeolepis clarki*, to the ecomorphological categories established by Mihalitsis et al. (2019) for extant piscivorous reefal teleosts. According to this categorization, actinopterygian mandibles can be front-fanged macrodont, back-fanged macrodont, or villiform/edentulous. Actinopterygians without large fangs on the mandible—possessing either many small, uniform teeth or no teeth at all—are categorized as villiform/edentulous. Their mandibles are hypothesized to be adapted for capturing and holding prey, including those with integumentary anti-predator defenses. Actinopterygians with large fangs on the mandible are distinguished based on the position of the largest fangs and interpreted based on lever mechanics. Actinopterygians with their largest fangs towards the anterior tip of the mandible are categorized as front-fanged macrodonts. Their fangs are hypothesized to be adapted for prey capture, but not processing, since their position away from the jaw joint (i.e., the fulcrum of the lever) means they rotate with high speed but low force. This produces a speed advantage. The smaller teeth posterior to the fangs are hypothesized to grip and cut prey. Actinopterygians with the largest fangs towards the posterior end of the mandible are categorized as back-fanged. Back-fanged macrodonts are the only ecomorphogical category hypothesized to be primarily adapted for prey processing by piercing, since the position of their largest fangs close to the jaw joint means they rotate with low speed but high force (i.e., a force advantage). The smaller teeth anterior to the largest fangs are hypothesized to be used in prey capture.

This categorization remains applicable for the non-neopterygian actinopterygians examined in this study despite significant phylogenetic distance and morphological differences between these and the reefal teleosts examined by Mihalitsis et al. (2019) because it relies on basic lever mechanics common to jaw closing (i.e., biting). The effect of the mode of prey capture and the identity of the elements making up the lower jaw should be minimal so long as the bite can be modeled as a lever rotating about a fulcrum. Indeed, Mihalitsis and Bellwood (2021) and Muruga et al. (2022) found that macrodont actinopterygians display a range of prey capture and processing behaviors. There are even broader functional differences between villiform Paleozoic actinopterygians and villiform teleosts with derived morphology enabling engulfing feeding behavior (Mihalitsis & Bellwood, 2019). However, villiform Paleozoic actinopterygians are still ecomorphologically distinct from macrodont Paleozoic actinopterygians even if they are not engulfers. Nevertheless, we focused on macrodont actinopterygians in this study to avoid this functional issue.

Mihalitsis and Bellwood (2021), Muruga et al. (2022), and related studies emphasize that behavioral observation and functional data should be considered in addition to ecomorphological data for a complete picture of organismal performance, niche, and the adaptive significance of morphology (Bock, 1977). As behavior cannot be observed for this specimen, we calculated a theoretical stress distribution to test for functional differences.

Theoretical Stress Distribution

We used the "functional homodonty" method of Cohen et al. (2020a, 2020b), in which tooth size and position estimate stress on the tooth and, since the stress exerted by a tooth influences its performance (Cohen et al., 2020b), establish differences in use. Calculating tooth stress using their method involves measuring the surface area of each tooth, determining the moment of force applied by each tooth (Formula 1), determining the stress experienced by each tooth (Formula 2), size-standardizing the stress (Formula 3), determining the residual stress for each tooth by subtracting the median from the size standardized stresses (Formula 4), and normalizing the residual stresses to the median (Formula 5) (Cohen et al., 2020a, 2020b). The formulae, with x = size standardized stress and $\tilde{x}$ = median stress, are:

$$\text{Formula 1: force} = \frac{(\text{distance from jaw tip to jaw joint}) * 1\text{N}}{(\text{distance from tooth tip to jaw joint})}$$

$$\text{Formula 2: theoretical stress (x)} = \frac{\text{Flever}}{\text{tooth surface area}}$$

$$\text{Formula 3: size standardized stress (x)} = \frac{\text{stress}}{\text{horizontal jaw length}^2}$$

$$\text{Formula 4: size standardized residual stress} = x - \tilde{x}$$

$$\text{Formula 5: median normalized residual stress} = \frac{\text{size standardized residual stress}}{\tilde{x}}$$

These formulae differ from the formulae published by Cohen et al. (2020a), which were misprinted in the proofing stage (K. Cohen, pers. comm.), but match the formulae contained in their fig. 1 (Cohen et al., 2020a). They also differ from the formulae published in the manuscript text of Cohen et al. (2020a), which take the reciprocal of Formula 1 and would yield the highest forces on the furthest teeth from the jaw joint and vice versa, which runs counter to basic lever mechanics (Mihalitsis & Bellwood, 2019) and their results. The order of operations listed here also differs from the order of operations published as a lettered list by Cohen et al. (2020a), which is incompatible with the order of operations stated elsewhere in the paper and their results.

We measured the jaw tip and tooth tip distances from 3D models of NSM 005.GF.045.260 (this paper) and *Austelliscus ferox* and *Tegeolepis clarki* (from Figueroa et al., 2021) using the measure function in MeshLab 2022.02. These specimens were broken, so the tip distances were measured from the point on the specimen closest to the presumed jaw joint (i.e., the most anterodorsal part of the specimen). This differed from the methodology of Cohen et al. (2020a, 2020b), which considered complete jaws, and would bias the analysis towards higher absolute forces applied to teeth. However, this effect is mitigated because the analysis considers relative differences between tooth stress and the position of the tooth relative to the tip length of the specimen. Relative, not absolute, values form the basis for comparison between teeth and between taxa. Additionally, we only considered well-preserved teeth in the lingual row for this study and excluded broken or damaged teeth. The functional homodonty method is robust to the removal of damaged teeth and our results remain comparable to those of Cohen et al. (2020a). Cohen et al. (2020a) only considered teeth that were fully ankylosed to the jaw, thus excluding all teeth undergoing replacement, so their method was designed to be robust to tooth exclusion. Both extant and fossil fishes may break or lose teeth during their lives; fossil specimens may additionally suffer taphonomic tooth damage or loss. Differences in the source of tooth damage should not bias our results, although we should expect to see a higher rate of tooth damage in fossil specimens because of the opportunity for

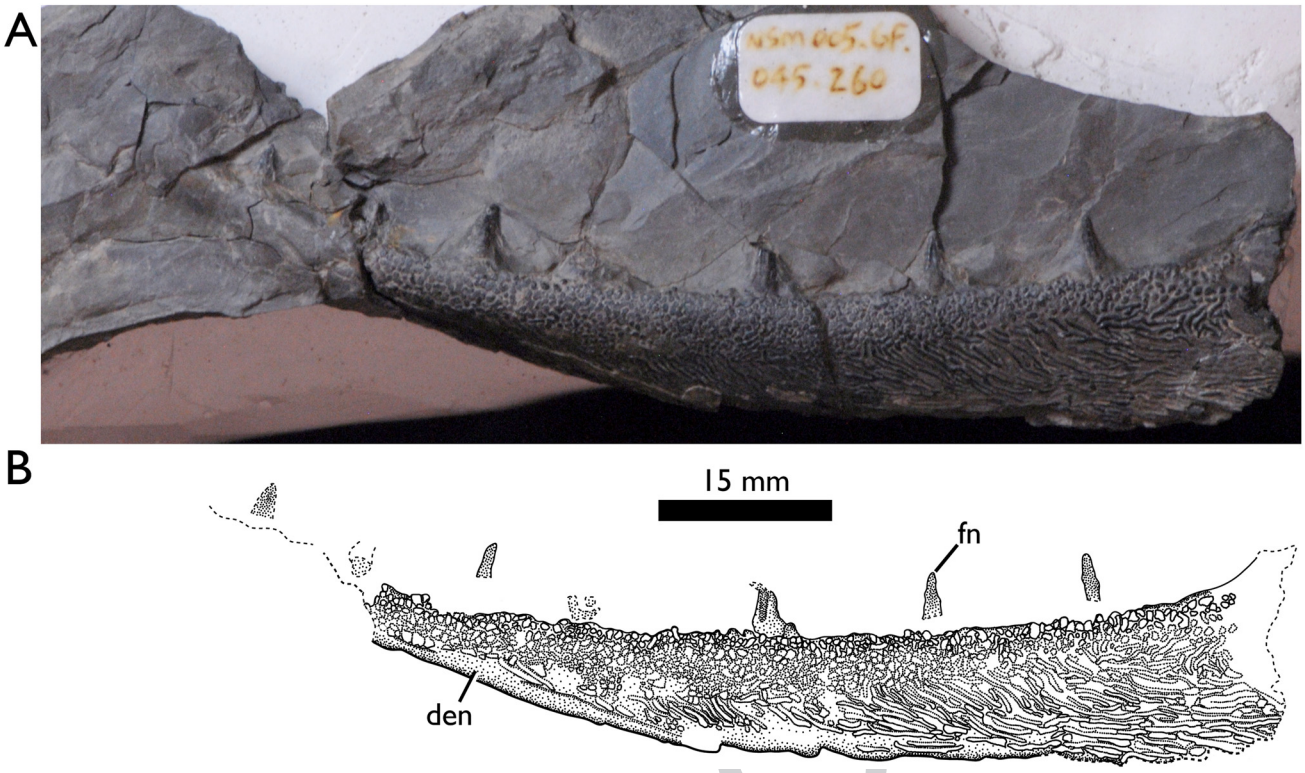

FIGURE 2. *Sphyragnathus tyche* gen. et sp. nov., NSM 005.GF.045.260. **A**, photograph and **B**, illustration of specimen in lateral view. **Abbreviations**: **den**, dentary; **fn**, fang. Scale bar equals 15 mm.

taphonomic damage. We only examined specimens with less than 50% of teeth broken and with sufficient tooth coverage to be representative of the overall dentition.

Paleozoic actinopterygians, including these taxa, have a marginal dentition (Giles et al., 2017) in addition to their primary dentary tooth row. We did not measure the marginal dentition as their small size, position, and likely functional role (Frazzetta, 1988) suggest that they are not primarily involved in biting and experience a different force regime. We calculated the surface area of each measured tooth by iteratively deleting all voxels except for the tooth being measured, calculating the surface area for the remaining mesh (i.e., the tooth being measured), and dividing the surface area by two (since the remaining meshes were hollow and open at the bottom).

We then calculated the median normalized residual stresses for each tooth preserved in NSM 005.GF.045.260, *Austelliscus ferox*, and *Tegeolepis clarki* according to our Formulae 1–4 in RStudio 2023.06.0 Build 421 (RStudio Team, 2024) running R. 4.3.1 (R Core Team, 2024) (Supplementary File 4, 5, and 6). We used the median normalized residual stress cutoff value of 4.3, established by Cohen et al. (2020a), to identify functionally heterodont teeth. That is, teeth that receive 4.3 times above the median stress for the dentition were found to be functionally different (Cohen et al., 2020a). We used this value rather than the lower value of 1.8 obtained by Cohen et al. (2020b) because the latter was targeted to a single genus (*Halichoeres* spp.), whereas the former considered multiple fish groups (Cohen et al., 2020a).

Institutional Abbreviations—**NSM**, Nova Scotia Museum of Natural History, Halifax, Nova Scotia; **RM**, Redpath Museum, McGill University, Montreal, Quebec.

SYSTEMATIC PALEONTOLOGY

OSTEICHTHYES Huxley, 1880
ACTINOPTERYGII Cope, 1889
SPHYRAGNATHUS TYCHE, gen. et sp. nov.
(Figs. 2–5)

Holotype—NSM 005.GF.045.260 was the primary focus, and initiator, of this study. It comprises the anterior part of an actinopterygian mandible, including the dentary and a set of coronoids that cannot be individually distinguished.

Examined Specimens—Recently, we examined all actinopterygian material in the collections of the Blue Beach Fossil Museum, NSM, and RM for mandibles similar to NSM 005.GF.045.260. We identified three specimens: NSM 007.GF.004.812, 005.GF.045.263, and 005.GF.045.367. These include the interior cast of a left dentary outlined by dentary and tooth fragments, a fragmentary dentary and partial cast of a left dentary, and the interior cast of a right dentary, respectively. The block identified as NSM 007.GF.004.812 also includes the impression of a large hyomandibula. Similarly, the block identified as NSM 005.GF.045.367 includes a second, straight dentary belonging to a different morphotype. Only the curved mandibles on these blocks were considered in this study; specimens were collected from a densely fossiliferous layer and the additional material is disarticulated and only loosely associated.

We also examined the holotype of *Acrolepis 'hortonensis'*, RM 2707, for comparison. RM 2707 represents a symphyseal fragment from an actinopterygian dentary bearing large fangs and an associated scale (Dawson, 1868; Gardiner, 1966).

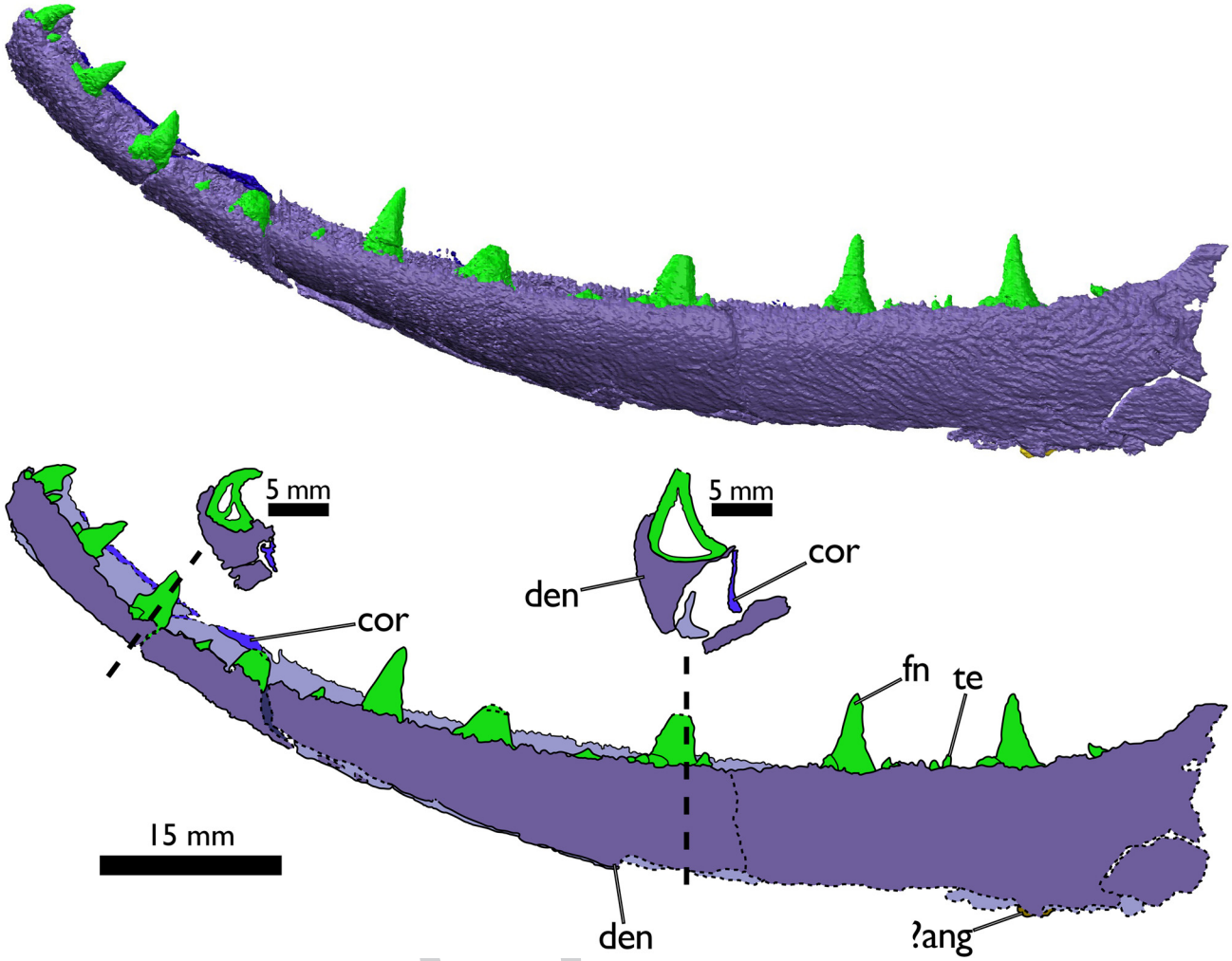

FIGURE 3. μCT rendering (top) and interpretative drawing (bottom) of *Sphyragnathus tyche* gen. et sp. nov., NSM 005.GF.045.260. in lateral view. **Abbreviations**: **?ang**, angular (gold); **cor**, coronoid (dark blue); **den**, dentary (purple); **fn**, fang (green); **te**, marginal dentition (green).

Etymology—Generic name, *Sphyragnathus*: Sphyra, hammer (σφῦρα, Greek); and *gnathus,* jaw (γνᾰθος, latinized Greek). Alludes to the inferred predatory nature of the taxon.

Specific name, *tyche*: Refers to the ancient Greek goddess of fortune, Tyche, for the fortunate circumstances of the fossil's discovery.

Diagnosis—*Sphyragnathus tyche* is identified as actinopterygian based on the presence of the mandibular canal in the dentary, the organization of teeth into two rows consisting of lingual fangs and marginal teeth, and vermiform ornamentation of glossy hypermineralized tubercles. *Sphyragnathus tyche* differs from other Paleozoic actinopterygians by the high degree of curvature of the mandible, the pattern of morphological heterodonty (small, curved teeth anteriorly grading into large erect teeth), and the substantial ventral deepening of the dentary in its posterior extent.

Locality, Horizon, and Age—All fossils examined in this study were collected from Tournaisian-aged (Tn2–Tn3 palynomorph stage) outcrops of the Horton Bluff Formation at the Blue Beach locality (Martel et al., 1993). NSM 005.GF.045.367, 007.GF.004.812, and 005.GF.045.263 were recovered among undifferentiated tidal debris along the western bank of the Avon River, so no specific horizon can be defined for these specimens (Anderson et al., 2015; Mansky & Lucas, 2013). NSM 005.GF.045.260 was discovered *in situ* by Sonja Wood and CFM in a creek along the Blue Beach Road as it approaches the Blue Beach Fossil Museum. These rocks are among the southernmost outcrops at the Blue Beach locality and form the base of the exposed section (Fig. 1) (Anderson et al., 2015; Mansky & Lucas, 2013). Thus, NSM 005.GF.045.260 can be confidently placed in the Blue Beach Member of the HBF as one of the oldest specimens discovered at the Blue Beach locality.

Description of NSM 005.GF.045.260

General Comments—The mandible is long, slender, and deeply curved with a dentition of large, heterodont fangs. The preserved length of the mandible is 101.11 mm. The mandible is curved along its entire length with its deepest curvature in the anterior half. The anterior-most point of the dentary is 23.60 mm above the plane of the lowest point along the dentary's dorsal margin.

Dentary—The dentary extends the entire preserved length of the specimen. It is broken into two pieces by a crack running the length of the specimen (Figs. 2, 3, 4, 5); the ventral lamina of the

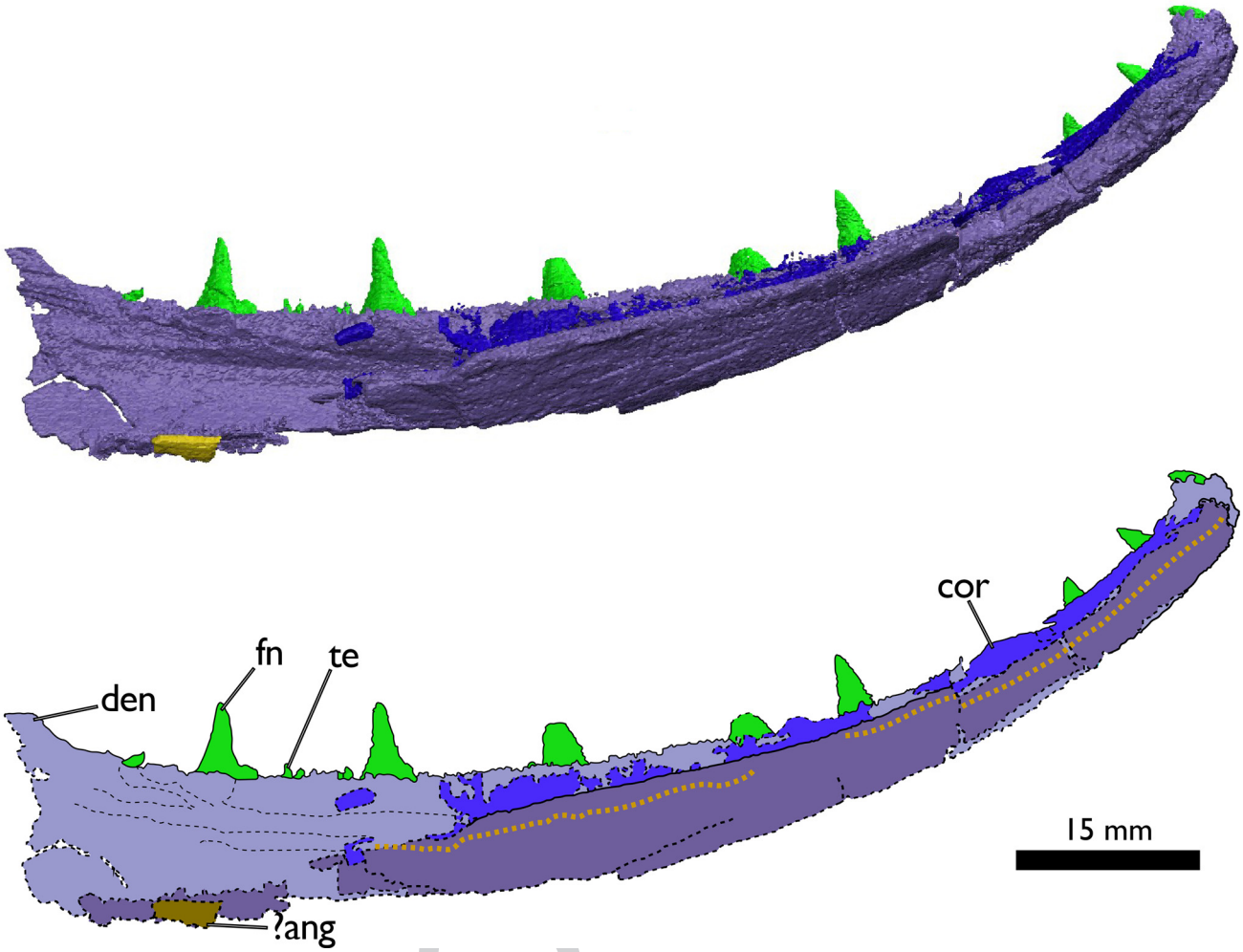

FIGURE 4. μCT rendering (top) and interpretative drawing (bottom) of *Sphyragnathus tyche* gen. et sp. nov., NSM 005.GF.045.260. in medial view. **Abbreviations**: **?ang**, angular (gold); cor, coronoid (dark blue); **den**, dentary (purple); **fn**, fang (green); **te**, marginal dentition (green). Position of mandibular canal indicated by thick, yellow dashed line.

dentary is folded inwards below the dorsal surface. Because of the breakage and folding, the thickened ventral part of the dentary carrying the mandibular canal has been pushed upwards so that it is at the same level as the dentition (Fig. 3). However, the preservation of the mandibular canal (Figs. 4, 5) suggests that the dentary is mostly complete in its ventral extent, at least posteriorly. An additional fragmented part of the ventral lamina is pushed anteriorly and overlaps the two other broken parts of the dentary medially (Figs. 3, 5A). The distinct rise in the dorsal margin of the dentary just ahead of the breakage at the posterior end likely marks the beginning of the rise in the mandible towards the elevated mandibular articular region common to large macrodont Paleozoic actinopterygians (Friedman et al., 2024) (Figs. 2, 3). The dentary is shortest and widest anteriorly, where it forms a thick rounded triangle in cross section, but becomes significantly taller and narrower posteriorly (Fig. 3). This gives it a tear-drop aspect in cross section in the middle part of its length before becomes more upright and laminar in its posterior-most extent (Fig. 3).

The convex labial surface of the dentary is well-ornamented with a glossy hyper-mineralized tissue (Fig. 2). Round tubercles are concentrated along the dorsal margin of the labial surface but lengthen into vermiform ridges ventrally (Fig. 2).

The dorsal surface of the dentary bears two rows of teeth between the small vertical external and internal laminae (Figs. 2, 5A). The labial row is the marginal dentition: this comprises small conical teeth set in the external lamina of the dentary, immediately next to the much larger lingual row of teeth. The lingual row features 25 tooth sockets; 16 empty and 9 set with teeth (Fig. 5A). The posterior-most socket is empty and is compressed relative to the others in series. The socket tapers posteriorly, bringing the external and internal laminae closer together (Fig. 5A). These laminae appear to be confluent posterior to this socket, suggesting it was the last in the row before the anterior margin of the adductor fossa (Fig. 5A).

The large lingual teeth vary considerably in size and shape. The smallest teeth are located symphyseally and are also the most curved, almost to the point of appearing doubled over (Figs. 3, 5A). The greatest degree of curvature is found in the third most anterior tooth (Fig. 5A). The degree of curvature gradually decreases in more posterior teeth, so the teeth at the posterior end of the specimen are nearly straight (Figs. 2, 3, 5A). All teeth are curved inward (i.e., point lingually) except two at the anterior end. The anterior-most tooth points posteriorly and the next tooth in series points

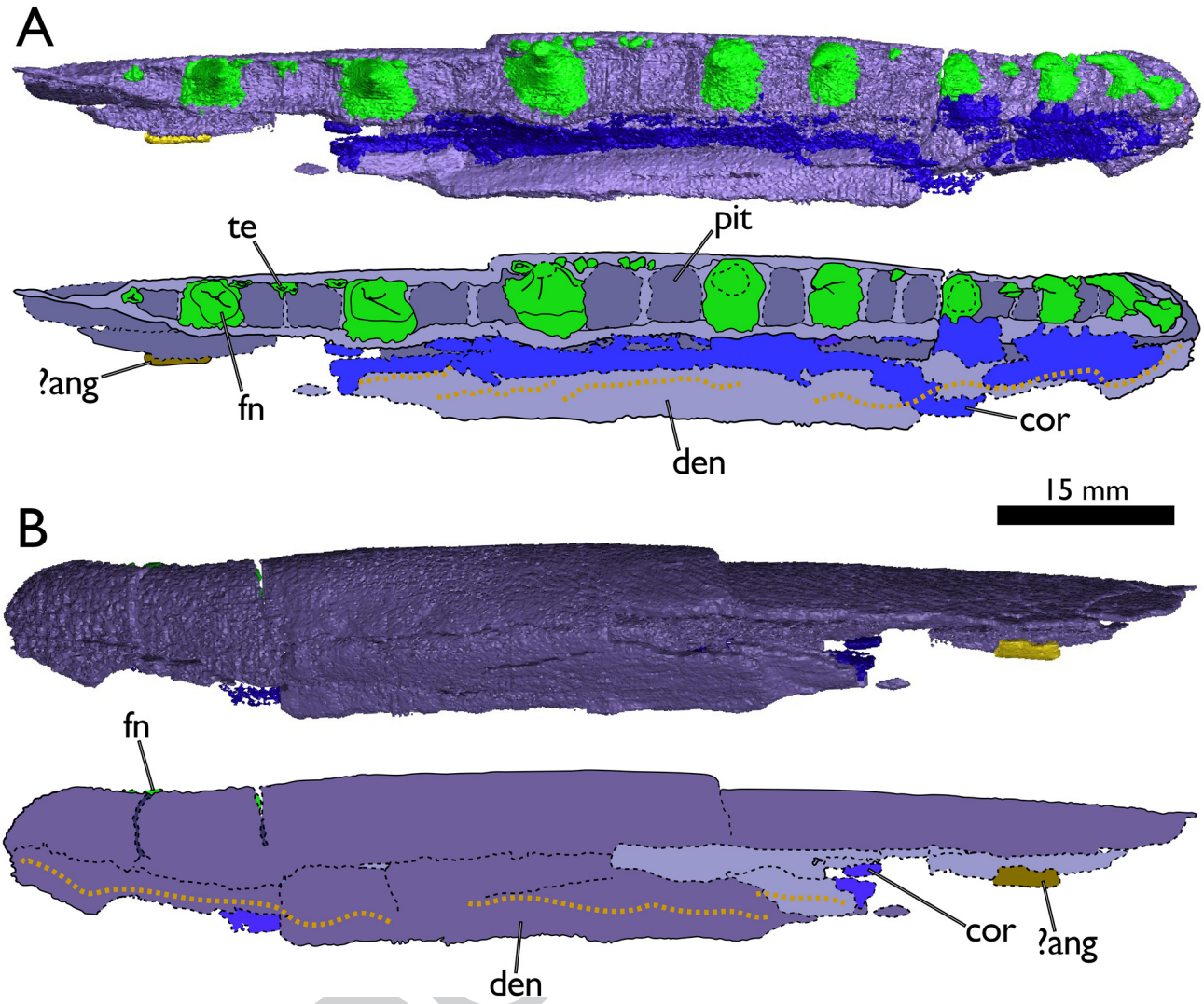

FIGURE 5. μCT renderings (top) and interpretative drawings (bottom) of *Sphyragnathus tyche* gen. et sp. nov., NSM 005.GF.045.260. in **A**, dorsal and **B**, ventral view. **Abbreviations**: **?ang**, angular (gold); **cor**, coronoid (dark blue); **den**, dentary (purple); **fn**, fang (green); **pit**, replacement pit; **te**, marginal dentition (green). Position of mandibular canal indicated by thick, yellow dashed line.

posteromedially, rotated halfway between the orientation of the anterior-most tooth and the more posterior teeth in the series (Fig. 5A). Although more posteriorly located teeth are always larger than the small and highly curved anterior teeth, the third tooth from the end of the specimen has the greatest diameter and height. These large teeth are partially accommodated by a small, thin shelf formed by the internal lamina of the dentary (Fig. 5A). However, the lamina curves around the base of the tooth and ascends, obscuring its base in medial view (Figs. 4, 5A).

Coronoids—The dentary is contacted along the dorsal margin of its lingual surface by a thin, incomplete, and displaced coronoid series (Figs. 4, 5A); these become more complete towards the anterior tip of the specimen. Individual coronoid bones cannot be distinguished. The labial edge of the coronoid series rests on the internal lamina of the dentary. The series has collapsed and fallen ventrally along most of its length so that its labial edge contacts the thickening for the mandibular canal on the broken and folded up ventral lamina (Figs. 3, 4, 5A). There is no evidence for the presence of fangs on the coronoid series; we consider this to be more likely due to biological absence rather than taphonomic damage.

Angular—A small fleck of bone in the posteroventral part of the specimen, lateral to the dentary, may represent a broken portion of the angular (Figs. 3, 4, 5).

Description of NSM 007.GF.004.812

General Comments—NSM 007.GF.004.812 comprises a partial internal cast of a left dentary surrounded by dentary fragments. The central part of the specimen appears as a curved cone marked by parallel lines. The impression of a single, large, posterior tooth protrudes from its dorsal surface. Small fragments of dentary fossil material appear below the cast; the largest, towards the middle of the specimen, bears the impression of the mandibular canal. The overall outline of the dentary appears elongate and curved (Fig. 6A).

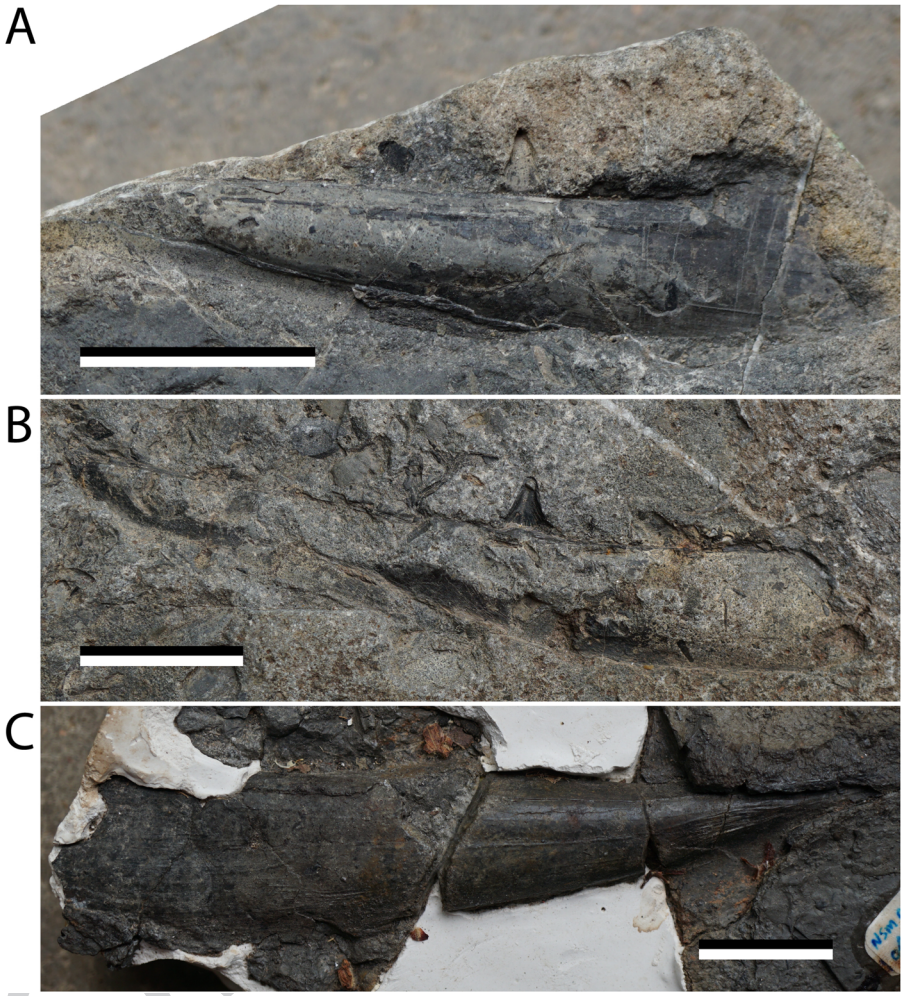

FIGURE 6. Large, curved, actinopterygian dentaries from the Blue Beach locality. **A**, NSM 007.GF.004.812, internal mold of actinopterygian left dentary and tooth impression surrounded by dentary fragments in left lateral view; **B**, NSM 005.GF.045.367, partial internal mold of actinopterygian left dentary outlined by dentary and tooth fragments; **C**, NSM 005.GF.045.263, internal mold of actinopterygian left dentary. Scale bars equal 2 cm.

Description of NSM 005.GF.045.367

General Comments—NSM 005.GF.045.367 comprises a partial internal cast of a left dentary outlined by dentary fragments; the largest fragments are in the posterior portion. Two large posterior teeth extend above the dorsal margin. The dentary appears slender, elongate, and curved (Fig. 6B).

Description of NSM 005.GF.045.263

General Comments—NSM 005.GF.045.263 appears as a curved cone marked by parallel lines representing an internal cast of a right dentary. This specimen appears relatively less curved than the others examined. The dentary outline appears relatively tall posteriorly and tapers significantly in its anterior extent (Fig. 6C).

Size Estimates

The total length estimate calculated for *Sphyragnathus tyche* (based on NSM 005.GF.045.260) following Figueroa et al. (2021) was 76.10–97.27 cm (Fig. 7). The standard length estimates calculated for *Sphyragnathus tyche* (based on NSM 005.GF.045.260), *Austelliscus ferox*, *Howqualepis rostridens*, and *Tegeolepis clarki* based on the data of Giles et al. (2023) were 45.85, 32.22, 29.94, and 84.80 cm, respectively (Supplementary File 3). These correspond to 95% prediction intervals of 39.60–52.10, 26.66–37.79, 24.46–35.42, and 75.62–94.07 cm, respectively (Fig. 7; Supplementary File 3).

Ecomorphological Categorization

The large fangs at the posterior end of the mandible establish *Sphyragnathus tyche* as a back-fanged macrodont (Figs. 2–5, 8); the large fangs towards the mandibular symphysis (Dunkle & Schaeffer, 1973; Figueroa et al., 2021) establish *Austelliscus ferox* and *Tegeolepis clarki* as front-fanged macrodonts (Fig. 8).

Theoretical Stress Distribution

The median normalized residual stresses ranged from −0.634 to 7.910 for *Austelliscus ferox*, −0.776 to 5.203 for *Tegeolepis clarki*, and −0.470 to 1.305 for *Sphyragnathus tyche* (Fig. 8, Supplementary File 6). The highest median normalized residual stresses were found in the posterior-most parts of the jaw and generally decreased anteriorly (Fig. 8, Supplementary File 6), matching the general decrease in force exerted on the teeth as calculated from basic lever mechanics (Supplementary File 6). The only median normalized residual stresses above the threshold of 4.3 established by Cohen et al. (2020) were found for the two most posterior teeth of *Austelliscus ferox* (7.910 and 5.775) and the most posterior tooth of *Tegeolepis clarki* (5.203) (Fig. 8, Supplementary File 6).

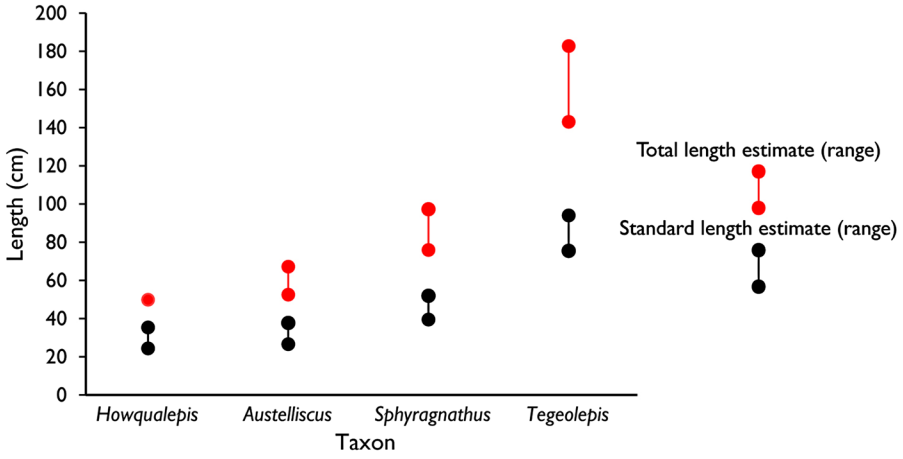

FIGURE 7. Standard length estimate results, in cm, for *Howqualepis rostridens*, *Austelliscus ferox*, *Sphyragnathus tyche*, and *Tegeolepis clarki*, and total length estimate results, in cm, for *Austelliscus ferox*, *Sphyragnathus tyche*, and *Tegeolepis clarki*. The total length data point for *Howqualepis rostridens* is derived from a direct measurement taken by Figueroa et al. (2021). Total length estimates are in red, standard length estimates are in black.

DISCUSSION

Morphology and Phylogeny

Status of *Sphyragnathus tyche* as an Actinopterygian—Morphological evidence indicates *Sphyragnathus tyche* is an actinopterygian. The presence of the mandibular canal within the dentary is characteristic of actinopterygians (Figueroa et al., 2021; Gardiner, 1984; Stensio, 1947). The state of other characters, such as the pattern of glossy hypermineralized ornamentation and the organized double row of lingual fangs and marginal teeth add confidence to this assessment (Figs. 2, 3).

Phylogenetic Position of *Sphyragnathus tyche* within Actinopterygii—Figueroa et al. (2019) discussed the problem of evaluating the relationships between actinopterygians with conspicuous predatory adaptations. Large teeth and elongate jaws—the ecomorphological hallmarks of predation in actinopterygians (Barnett et al., 2006; Wainwright & Bellwood, 2002)—have repeatedly formed the basis for dubious taxonomic groupings (e.g., Acrolepidae, Cosmoptychiidae, Pygopteridae, and Rhabdolepidae). The fossil record of Carboniferous–Permian large macrodont actinopterygians was also reviewed by Friedman et al. (2024) in a study which introduced considerable new μCT data and anatomical understanding for mandibles from these taxa. However, the relationships of Paleozoic macrodont actinopterygians have not generally been tested in phylogenetic analyses (Figueroa et al., 2019).

Despite superficial morphological similarity, there is no apparent relationship between *Sphyragnathus tyche* and *Austelliscus ferox* + *Tegeolepis clarki* because it lacks the synapomorphies of these taxa. Notably, *Sphyragnathus tyche* lacks a constriction of the mandible before its anterior tip as in *Austelliscus ferox* (Figueroa et al., 2019), and the jaw is continuously curved, not reflexed solely at its anterior tip (Figs. 2, 3, 4). The size, shape, and position of teeth also differ. *Austelliscus ferox* and *Tegeolepis clarki* are front-fanged macrodonts with conical teeth that are anteriorly inclined at the posterior of the jaw, but *Sphyragnathus tyche* is a back-fanged macrodont with deeply curved anterior teeth that become conical and upright posteriorly.

Assessing the relationship between *Sphyragnathus tyche* and post-Devonian actinopterygians is more difficult. It shares morphological characters in the mandible and dentition with these taxa: the mandible rises dorsally, presumably towards an elevated articular surface common to large Paleozoic macrodont actinopterygians, and the anterior dentition is curved inwards towards the lingual side of the jaw as in these taxa (Friedman et al., 2024). The extreme curvature of the lower jaw combined with the pattern of morphological heterodonty in *Sphyragnathus tyche* distinguish it from the known morphological diversity for these broader taxa. *Sphyragnathus tyche* appears somewhat similar to the lower jaws of *Brazilichthys macrognathus*, *Daemodontiscus harrisae*, and *Watsonichthys pectinatus* but is deeper in profile, more deeply curved, and has a different dentition. These apomorphies may distinguish *Sphyragnathus tyche* from these taxa, but *Sphyragnathus tyche* critically lacks synapomorphies with any well-defined actinopterygian group. Broader reassessment of the relationships of Paleozoic actinopterygians will be necessary to further elucidate the relationship between *Sphyragnathus tyche* and ecomorphologically similar forms.

Macrodont Actinopterygians at the Blue Beach Locality—The actinopterygian mandibles described here represent only part of the mandibular morphological diversity at the Blue Beach locality. Our survey revealed abundant large mandibles with diverse morphology incompatible with *Sphyragnathus tyche*. These will be discussed in a planned review of the Horton Bluff Formation fish fauna. *Acrolepis* '*hortonensis*' (Fig. 9) is clearly distinct from *Sphyragnathus tyche*—the profile of the dentary is straight in its anterior extant and it bears large, straight fangs suggestive of front-fanged macrodonty (Fig. 9). This taxon appears in need of revision, but this is beyond the scope of this work.

NSM 007.GF.004.812, 005.GF.045.367, and 005.GF.045.263 (Fig. 6A, B, C, respectively) are too incomplete to act as paratypes for or be confidently referred to *Sphyragnathus tyche*. However, they match the morphotype of *Sphyragnathus tyche*. Large fangs in the posterior part of NSM 007.GF.004.812 and 005.GF.045.263 are compatible with back-fanged macrodonty.

Overall, large actinopterygians with conspicuous predatory adaptations are a significant and diverse component of the Blue Beach assemblage. This observation is compatible with the head-first/feeding-first hypothesis, but we emphasize that this cannot be tested fully without post-cranial data.

Ecology and Functional Morphology

Size Estimates—Because the mandibles of *Sphyragnathus tyche* and *Austelliscus ferox* used for measurement were incomplete, the 95% prediction intervals calculated for standard length—39.60–52.10 cm and 26.66–37.79 cm respectively—represent a range of minimum possible standard lengths (Fig. 7). The mandible of *Howqualepis rostridens* and *Tegeolepis clarki* used for the calculation were complete, so the range of standard length estimates for these taxa (24.46–35.42 cm and 75.62–94.07 cm, respectively; Fig. 6) represent both minimum and maximum values. Since this should bias *Howqualepis rostridens*

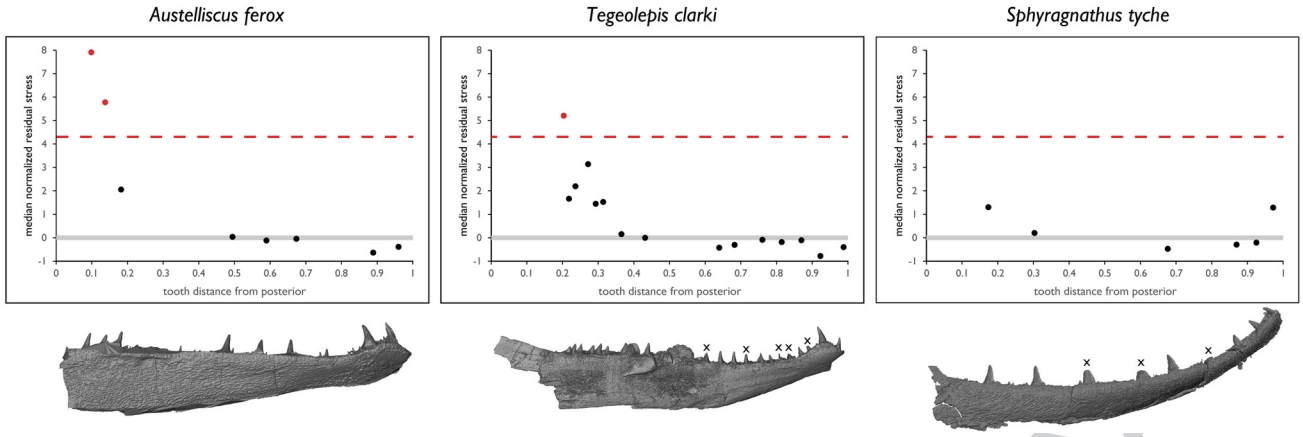

FIGURE 8. Results of theoretical stress distribution analysis for *Austelliscus ferox*, *Tegeolepis clarki*, and *Sphyragnathus tyche*. Values for stress are given as median normalized residuals. Tooth distance from posterior was determined as the ratio between the distance from the posterodorsal corner of the mandible to the tip of each tooth and the distance from the distal tip of the mandible to its posterodorsal corner. The solid gray line represents a residual stress of 0 (i.e., the median stress for the dentition). The red dashed line represents the functional homodonty threshold value of 4.3 (Cohen et al., 2020a), data points for median normalized residual stress exceeding this threshold are also colored red. Images below each graph are µCT-based renderings of the mandibles used for measurement. 'X's above teeth indicate teeth that were not used for measurement due to their incompleteness.

towards larger size relative to the taxa for which only minimums were calculated, this reinforces our estimate of *Howqualepis rostridens* as the smallest of the taxa measured.

Our absolute minimum total length estimate for *Sphyragnathus tyche* (76.10 cm) places it as the second largest actinopterygian in the dataset of Sallan and Galimberti (2015). Our 'maximum minimum' total length estimate (97.27 cm) closely approaches the total length cited for *Tegeolepis clarki* (100 cm), the largest actinopterygian in the dataset (Fig. 7) (Sallan & Galimberti, 2015).

We consider our standard length estimates to be more robust than our total length estimates, since they are based on direct measurements from fossils or figures of fossils (Giles et al., 2023), rather than lateral reconstructions (Figueroa et al., 2021). These corroborate our total length results by estimating the same relative sizes for each taxon (i.e., *Austelliscus ferox* < *Sphyragnathus tyche* < *Tegeolepis clarki*; Fig. 7).

Thus, *Sphyragnathus tyche* is one of the largest actinopterygians known from the Devonian and early Carboniferous periods and provides evidence large, predatory actinopterygians were present on either side of the Hangenberg extinction boundary. This observation runs counter to the decrease in body size hypothesized for this interval by Sallan and Galimberti (2015) but is compatible with the results of Giles et al. (2023), who did not find such a decrease in actinopterygian body size.

Ecomorphological Categorization—The early Carboniferous *Sphyragnathus tyche* is the earliest occurrence of a back-fanged macrodont in the actinopterygian fossil record. According to the interpretation of these categories by Mihalitsis et al. (2019), this suggests that *Sphyragnathus tyche* is the earliest known actinopterygian with a mandible with adaptations for prey processing by piercing as well as prey capture. The shape of the teeth in *Sphyragnathus tyche* is compatible with this interpretation. The deep inward curvature of the anterior teeth would make it difficult for prey to escape outwards (Figs. 3–5) and the upright conical posterior teeth appear suited to a role in processing prey via piercing. This inferred difference in feeding strategy furthers the expectation that *Sphyragnathus tyche* should have a different theoretical stress distribution than the Devonian taxa examined.

Theoretical Stress Distribution—This prediction is supported by the theoretical stress distribution. Whereas stresses appear evenly distributed across the dentition of *Sphyragnathus tyche*, the posterior-most teeth of *Austelliscus ferox* and *Tegeolepis clarki* experience stresses several times above the median stress for the dentition (Fig. 8), exceeding the threshold for functional heterodonty established by Cohen et al. (2020). Conversely, *Sphyragnathus tyche* is a functional homodont according to their published criteria implying that all teeth in the dentition are functionally similar (Fig. 8).

We challenge this interpretation of functional homodonty in *Sphyragnathus tyche* because the method of Cohen et al. (2020a, 2020b) only identifies teeth that experience distinctly high levels of stress. It cannot identify those that experience distinctly low levels of stress, which Cohen et al. (2020a) agree should also be considered functionally heterodont. Although the negative normalized residual stress threshold for functional heterodonty (−4.3) implies that low-stress can be identified, a median normalized residual stress lower than −1 is impossible. Combining Formula 3 (residual stress = $x - \tilde{x}$) and Formula 4 (median normalized residual stress = $\frac{\text{residual stress}}{\tilde{x}}$), where x = size standardized stress and $\tilde{x}$ = the median stress for the dentition, yields Formula 5:

$$\text{median normalized residual stress} = \frac{x - \tilde{x}}{\tilde{x}}$$

The lowest possible value for stress is 0, since negative stress cannot occur during biting. In this scenario, and assuming at least one other tooth in the dentition experiences stress (i.e., for $x = 0$ and $\tilde{x} > 0$):

$$\text{median normalized residual stress} = \frac{(0) - \tilde{x}}{\tilde{x}}$$

$$\text{median normalized residual stress} = \frac{-\tilde{x}}{\tilde{x}}$$

$$\text{median normalized residual stress} = -1$$

Furthermore, the −4.3 threshold is incompatible with the thresholding method. Cohen et al. (2020a) generated their

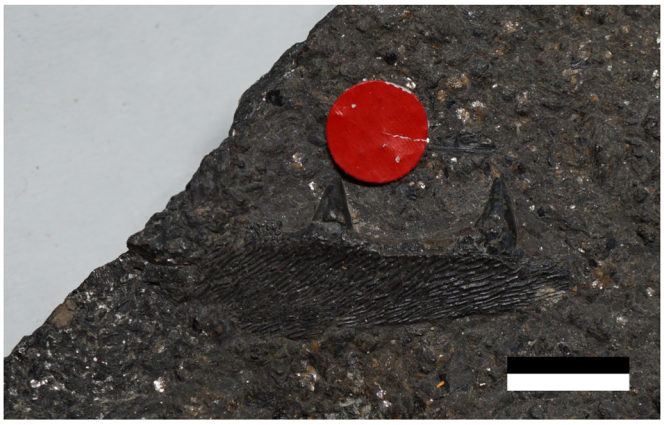

FIGURE 9. *Acrolepis 'hortonensis,'* RM 2707, right actinopterygian dentary in right lateral view. Scale bar equals 1 cm.

thresholds using k-means clustering, a technique that resolves data into a user-specified number of clusters, to identify the threshold. Cohen et al. (2020a) specified two clusters of bootstrapped residuals with average median normalized residual stress values of 0.1 for the low cluster (i.e., their functional homodonts) and 8.1 for the high cluster (i.e., their high-stress functional heterodonts). There was no cluster of teeth experiencing large negative values (i.e., low-stress functional heterodonts). The average between the two clusters determines the threshold (Cohen et al., 2020a) and this average is solely positive. This conclusion seems to be reflected in later work by Cohen et al. (2020a), who state only the positive value of their functional heterodonty threshold (i.e., + 1.8) in their study of *Halichoeres* spp. wrasses.

We argue that the functional heterodonty method of Cohen et al. (2020a, 2020b) captures only part of the functional heterodonty concept because it only identifies teeth experiencing distinctly high stress. Since the force advantage experienced by a tooth decreases with its distance from the jaw joint, and stress is the quotient of force and area, the functionally heterodont teeth identified are relatively small and set towards the posterior end of the jaw (see figs. 7 and 8 and supplementary figs. 2–5 in Cohen et al. [2020a] and fig. 4 in Cohen et al. [2020b]). Since front-fanged macrodonts are characterized by relatively small posterior teeth (Mihalitsis & Bellwood, 2019), they should be identified preferentially as functional heterodonts by this method. Back-fanged macrodonts, with their largest teeth in position to receive the highest forces (Mihalitsis & Bellwood, 2019), should not be identified as functional heterodonts by the method. This matches our results: the front-fanged macrodonts *Austelliscus ferox* and *Tegeolepis clarki* had teeth exceeding the functional heterodonty threshold, and the back-fanged macrodont *Sphyragnathus tyche* did not (Fig. 8).

The relative low median normalized residual stresses calculated for the posterior teeth of *Sphyragnathus tyche* (Fig. 8) are compatible with the use of these teeth inferred from the ecomorphological categorization. If back-fanged macrodonts, such as *Sphyragnathus tyche*, primarily use their posterior teeth for prey processing by piercing (Mihalitsis & Bellwood, 2019), it would be counterintuitive for these teeth to experience potentially damaging high levels of relative stress. Instead, the large size of these teeth likely provides a safety factor so that they experience less stress than their maximum tolerance (Lungstrom et al., 2023). The relatively low stresses experienced by the anterior teeth and the relatively high stresses experienced by the posterior teeth in the front-fanged macrodonts *Austelliscus ferox* and *Tegeolepis clarki* are also compatible with their inferred role in prey capture and prey gripping and cutting, respectively.

We suggest that a revision to the functional heterodonty method is necessary to capture the full functional heterodonty concept (Cohen et al., 2020a). However, it is sufficient for the research objectives of this paper to observe that the significant difference in the theoretical stress distributions of *Austelliscus ferox* and *Tegeolepis clarki* versus *Sphyragnathus tyche* matches our prediction and corroborates the ecomorphological categorization of these taxa.

The Devonian–Carboniferous Transition in Actinopterygians

The Feeding-first Hypothesis—Our ecomorphological categorization and analysis of theoretical stress distribution for *Austelliscus ferox*, *Sphyragnathus tyche*, and *Tegeolepis clarki* match our predictions. Important differences in the size and position of their teeth suggest they differ functionally. The tooth and mandibular morphology (back-fanged macrodonty) of *Sphyragnathus tyche* is a first for actinopterygians in the fossil record, as is its likely functional adaptation for prey-processing by piercing (Mihalitsis & Bellwood, 2019). The absence of any known post-cranial material means that *Sphyragnathus tyche* cannot provide data on the relative timing of cranial and postcranial morphological diversification or of functional changes related to feeding and locomotion. However, it provides a positive example of new cranial morphology related to feeding in early Carboniferous actinopterygians, as predicted by the feeding-first hypothesis. We suggest the broader early Carboniferous actinopterygian fauna overall remains more compatible with a morphologically neutral version of the feeding-first hypothesis. The earlier-than-expected appearance of deep-bodied actinopterygians runs against the central prediction of the head-first hypothesis but remains compatible with the feeding-first hypothesis (Wilson et al., 2021), since a deep body enables specific feeding behaviors in modern actinopterygians (Perevolotsky et al., 2020).

The proliferation of Carboniferous-aged deep-bodied actinopterygians may also be associated with the exploration of new prey types and ecological roles. At least two different groups of deep-bodied actinopterygian ('platysomids' and eurynotids (Friedman et al., 2018; Sallan & Coates, 2013) convergently developed blunt dentitions in the early Carboniferous period that probably represented adaptations for durophagy. Since the earliest known (Tournaisian) deep-bodied actinopterygian, a platysomid, preserves only its posterior half (Wilson et al., 2021) and the first blunt actinopterygian dentitions appear in Viséan deep-bodied actinopterygians (Friedman et al., 2018; Sallan & Coates, 2013), the relative timing of dentition and body-shape evolution in deep-bodied fishes is uncertain. Nevertheless, the first appearance of deep-bodied and blunt-toothed, and back-fanged macrodont actinopterygians supports the interpretation that the conspicuous morphological and functional diversification of Carboniferous actinopterygians represents adaptation for new patterns of prey use requiring specialized feeding strategies (e.g., crushing of benthic hard-bodied prey and capture and processing of elusive prey). Continued exploration of ecomorphology and functional morphology, including analytical testing of trait divergence, theoretical analysis and direct performance testing, should help build our understanding of ecological change in Devonian–Carboniferous actinopterygians more broadly.

CONCLUSION

NSM 005.GF.045.260 represents a new genus and species of actinopterygian, *Sphyragnathus tyche*, characterized by a long, curved jaw bearing large, upright fangs posteriorly and smaller

teeth anteriorly. *Sphyragnathus tyche* is the second largest actinopterygian known from Devonian and early Carboniferous times—larger than *Austelliscus ferox* but smaller than *Tegeolepis clarki*. Despite the superficial similarity in the shared presence of long jaws and large fangs of these three taxa, *Austelliscus ferox* and *Tegeolepis clarki* belong to different ecomorphological categories than *Sphyragnathus tyche* based on the size and position of their fangs. The different ecomorphological categories for these taxa suggest they used their jaws differently, which is borne out by significant differences in stress distribution across their dentitions. Taken together, these results contribute to an emerging picture of change in which early actinopterygians diversified cryptically in the Devonian, survived the Hangenberg extinction relatively unaffected, and quickly developed new morphologies in the Early Carboniferous as adaptations for feeding.

ACKNOWLEDGMENTS

First, we thank the late Sonja Wood (Blue Beach Fossil Museum). Sonja discovered NSM 005.GF.045.260 and facilitated our work at the BBFM. Sonja was dedicated to the BBFM and campaigned tirelessly to improve the lives of those who live in her region of Nova Scotia. She will be deeply missed. We thank A. Howell (RM), Tim Fedak (NSM), and K. Ogden (NSM) for specimen access and curatorial support. The work published here was discussed as a pilot project for a broader analysis of jaw function as part of CDW's PhD thesis proposal. We thank T. Miyashita for helpful discussions and critical feedback on the thesis proposal that was incorporated here. R. Figueroa, M. Mihalitsis, and K. Cohen kindly discussed their work and provided helpful suggestions. We also thank J. Pardo and H. Maddin, and our peer reviewers for helpful discussions and critical feedback. Research was supported by NSERC Discovery Grants 2017-04821 and 2023-04423 to Jason Anderson, and NSERC CGS M and CGS D (Alexander Graham Bell) awards to Conrad Wilson. Examination of additional material was supported by NSERC Discovery Grant RGPIN-06442 to H. Maddin.

AUTHOR CONTRIBUTIONS

CDW designed the project, gathered and analyzed the data, and drafted the manuscript, CFM collected and initially curated the specimen, and JSA arranged specimen access and laboratory analysis. All authors edited the manuscript.

DATA AVAILABILITY STATEMENT

All authored data needed to replicate this study are included in the Supplementary Files.

DISCLOSURE STATEMENT

No potential conflict of interest was reported by the author(s).

ORCID

Conrad D. Wilson http://orcid.org/0009-0000-8499-0213
Jason S. Anderson http://orcid.org/0000-0002-4503-8657

SUPPLEMENTARY FILES

Supplementary File 1.zip: archive containing the reconstructed image stack in .tiff format.

Supplementary File 2.ply: archive containing 3D model of NSM 005.GF.045.260 used for measurement in .ply format.

Supplementary File 3.xls: workbook for linear regression between jaw and body length and to generate body length forecasts.

Supplementary File 4.csv: dataset of raw measurements used to calculate theoretical stress distribution.

Supplementary File 5.zip: archive containing R script used to calculate theoretical stress distribution in .rmd format.

Supplementary File 6.xls: results of theoretical stress distribution and initial graphing.

LITERATURE CITED

Anderson, J. S., Smithson, T., Mansky, C. F., Meyer, T., & Clack, J. (2015). A Diverse Tetrapod Fauna at the Base of "Romer's Gap.". *PLOS One*, *10*(4), e0125446. https://doi.org/10.1371/journal.pone.0125446

Barnett, A., Bellwood, D. R., & Hoey, A. S. (2006). Trophic ecomorphology of cardinalfish. *Marine Ecology Progress Series*, *322*, 249–257. https://doi.org/10.3354/meps322249

Bock, W. J. (1977). Toward an ecological morphology. *Vogelwarte*, *29*, 127–135.

Camp, A. L., Olsen, A. M., Hernandez, L. P., & Brainerd, E. L. (2020). Fishes can use axial muscles as anchors or motors for powerful suction feeding. *Journal of Experimental Biology*, *223*(18), jeb225649. https://doi.org/10.1242/jeb.225649

Coates, M. I., & Tietjen, K. (2018). This strange little palaeoniscid": a new early actinopterygian genus, and commentary on pectoral fin conditions and function. *Earth and Environmental Science Transactions of the Royal Society of Edinburgh*, *109*(1–2), 15–31. https://doi.org/10.1017/S1755691018000403

Cohen, K. E., Weller, H. I., & Summers, A. P. (2020). Not your father's homodonty—stress, tooth shape, and the functional homodont. *Journal of Anatomy*, *237*(5), 837–848. https://doi.org/10.1111/joa.13248

Cohen, K. E., Weller, H. I., Westneat, M. W., & Summers, A. P. (2023). The Evolutionary Continuum of Functional Homodonty to Heterodonty in the Dentition of Halichoeres Wrasses. *Integrative And Comparative Biology*, *63*(1), 176–187. https://doi.org/10.1093/icb/icaa137 Q8

Collar, D. C., Wainwright, P. C., & Alfaro, M. E. (2008). Integrated diversification of locomotion and feeding in labrid fishes. *Biology Letters*, *4*(1), 84–86. https://doi.org/10.1098/rsbl.2007.0509 Q9

Cope, E. D. (1889). Geology and Palaeontology. *The American Naturalist*, *21*(11), 1014–1019. https://doi.org/10.1086/274979 Q10

Dawson, J. W. (1868). *The Geological Structure, Organic Remains, and Mineral Resources of Nova Scotia, New Brunswick, and Prince Edward Island*. Macmillan and Co.

Dunkle, D. H., & Schaeffer, B. (1973). *Tegeolepis clarki* (Newberry), a palaeonisciform from the upper Devonian Ohio shale. *Palaeontographica Abt. A*, *143*(1–6), 151–158.

Figueroa, R. T., Friedman, M., & Gallo, V. (2019). Cranial anatomy of the predatory actinopterygian *Brazilichthys macrognathus* from the Permian (Cisuralian) Pedra de Fogo Formation, Parnaíba Basin. *Journal of Vertebrate Paleontology*, *39*(3), e1639722. https://doi.org/10.1080/02724634.2019.1639722

Figueroa, R. T., Weinschütz, L. C., & Friedman, M. (2021). The oldest Devonian circumpolar ray-finned fish? *Biology Letters*, *17*(3), 20200766. https://doi.org/10.1098/rsbl.2020.0766

Fletcher, T., Altringham, J., Peakall, J., Wignall, P., & Dorrell, R. (2014). Hydrodynamics of fossil fishes. *Proceedings of the Royal Society B: Biological Sciences*, *281*(1788), 20140703. https://doi.org/10.1098/rspb.2014.0703

Frazzetta, T. H. (1988). The mechanics of cutting and the form of shark teeth (Chondrichthyes, Elasmobranchii). *Zoomorphology*, *108*(2), 93–107. https://doi.org/10.1007/BF00539785

Friedman, M., Figueroa, R. T., Hodnett, J.-P. M., Lucas, S. G., Higgins, R. R., Pierce, S., & Giles, S. (2024). A new genus and species of large macrodont actinopterygian from the Pennsylvanian (Kasimovian/Missourian) Atrasado Formation of New Mexico. *Contributions from the Museum of Paleontology, University of Michigan*, *36*(2), 1–36.

Friedman, M., Pierce, S. E., Coates, M., & Giles, S. (2018). Feeding structures in the ray-finned fish *Eurynotus crenatus* (Actinopterygii: Eurynotiformes): implications for trophic diversification among Carboniferous actinopterygians. *Earth and Environmental Science Transactions of the Royal Society of Edinburgh*, *109*(1–2), 33–47. https://doi.org/10.1017/S1755691018000816

Friedman, M., & Sallan, L. C. (2012). Five hundred million years of extinction and recovery: a phanerozoic survey of large-scale diversity patterns in fishes. *Palaeontology*, *55*(4), 707–742. https://doi.org/10.1111/j.1475-4983.2012.01165.x

Gans, C., & Northcutt, R. G. (1983). Neural Crest and the Origin of Vertebrates: A New Head. *Science*, *220*(4594), 268–273. doi:10.1126/science.220.4594.268

Gardiner, B. G. (1966). Catalogue of Canadian fossil fishes. *Life Sciences Royal Ontario Museum University of Toronto*, *68*, 1–154.

Gardiner, B. G. (1984). The relationships of the palaeoniscid fishes, a review based on new specimens of *Mimia* and *Moythomasia* from the Upper Devonian of Western Australia. *Bulletin of the British Museum of Natural History, Geology*, *37*(November), 173–428.

Giles, S., Feilich, K., Warnock, R. C. M., Pierce, S. E., & Friedman, M. (2023). A Late Devonian actinopterygian suggests high lineage survivorship across the end-Devonian mass extinction. *Nature Ecology & Evolution*, *7*(1), 10–19. https://doi.org/10.1038/s41559-022-01919-4

Giles, S., Xu, G.-H., Near, T. J., & Friedman, M. (2017). Early members of 'living fossil' lineage imply later origin of modern ray-finned fishes. *Nature*, *549*(7671), 265–268. https://doi.org/10.1038/nature23654

Henderson, S., Dunne, E. M., & Giles, S. (2022). Sampling biases obscure the early diversification of the largest living vertebrate group. *Proceedings of the Royal Society B: Biological Sciences*, *289*(1985), 20220916. https://doi.org/10.1098/rspb.2022.0916

Huxley, T. H. (1880). On the Application of the Laws of Evolution to the Arrangement of the Vertebrata, and more particularly of the Mammalia. *Proceedings of the Zoological Society of London*, *43*, 649–662.

Lauder, G. V. (1980). Evolution of the feeding mechanism in primitive actinopterygian fishes: A functional anatomical analysis of *Polypterus*, *Lepisosteus*, and *Amia*. *Journal of Morphology*, *163*(3), 283–317. https://doi.org/10.1002/jmor.1051630305

Lemberg, J. B., Shubin, N. H., & Westneat, M. W. (2019). Feeding kinematics and morphology of the alligator gar (Atractosteus spatula, Lacépède, 1803). *Journal of Morphology*, *280*(10), 1548–1570. https://doi.org/10.1002/jmor.21048

Li, E. Y., Kaczmarek, E. B., Olsen, A. M., Brainerd, E. L., & Camp, A. L. (2022). Royal knifefish generate powerful suction feeding through large neurocranial elevation and high epaxial muscle power. *Journal of Experimental Biology*, *225*(11), jeb244294. https://doi.org/10.1242/jeb.244294

Long, J. A. (1988). New palaeoniscoid fishes from the Late Devonian and Early Carboniferous of Victoria. *Memoirs of the Association of Australasian Palaeontologists*, *7*, 1–64.

Lungstrom, L., Westneat, M., Huie, J., Kolmann, M., & Cohen, K. (2023). Sink your teeth into the Puncture Performance of a Payara Pendulum. *Society of Integrative and Comparative Biology*.

Mansky, C. F., & Lucas, S. G. (2013). Romer's Gap revisited: continental assemblages and ichno-assemblages from the basal Carboniferous of Blue Beach, Nova Scotia, Canada. In S. G. Lucas, W. A. DiMichele, J. E. Barrick, J. W. Schneider, & J. A. Spielmann (Eds.), *Bulletin 60: The Carboniferous-Permian Transition* (pp. 244–273). New Mexico Museum of Natural History and Science.

Martel, A. T., & Gibling, M. R. (1991). Wave-dominated lacustrine facies and tectonically controlled cyclicity in the Lower Carboniferous Horton Bluff Formation, Nova Scotia, Canada. *Special Publications of the International Association of Sedimentologists*, *13*, 223–243.

Martel, A. T., & Gibling, M. R. (1996). Stratigraphy and tectonic history of the Upper Devonian to Lower Carboniferous Horton Bluff Formation, Nova Scotia. *Atlantic Geology*, *32*(1), 13–38. doi:10.4138/2076

Martel, A. T., McGregor, D. C., & Utting, J. (1993). Stratigraphic significance of Upper Devonian and Lower Carboniferous miospores from the type area of the Horton Group, Nova Scotia. *Canadian Journal of Earth Sciences*, *30*(5), 1091–1098. https://doi.org/10.1139/e93-092

Mihalitsis, M., & Bellwood, D. (2019). Functional implications of dentition-based morphotypes in piscivorous fishes. *Royal Society Open Science*, *6*(9), 190040. https://doi.org/10.1098/rsos.190040

Mihalitsis, M., & Bellwood, D. R. (2021). Functional groups in piscivorous fishes. *Ecology and Evolution*, *11*(18), 12765–12778. https://doi.org/10.1002/ece3.8020

Muruga, P., Bellwood, D. R., & Mihalitsis, M. (2022). Forensic odontology: Assessing bite wounds to determine the role of teeth in piscivorous fishes. *Integrative Organismal Biology*, *4*(1), https://doi.org/10.1093/iob/obac011

Perevolotsky, T., Martin, C. H., Rivlin, A., & Holzman, R. (2020). Work that body: fin and body movements determine herbivore feeding performance within the natural reef environment. *Proceedings of the Royal Society B: Biological Sciences*, *287*(1938), 20201903. https://doi.org/10.1098/rspb.2020.1903

R Core Team (2024). *R: A language and environment for statistical computing*. https://www.r-project.org

Rice, A. N., & Hale, M. E. (2010). Roles of Locomotion in Feeding. In P. Domenici, & B. G. Kapoor (Eds.), *Fish Locomotion: An Eco-ethological Perspective* (pp. 171–199). Science Publishers.

RStudio Team. (2024). *RStudio: Integrated Development for R*. RStudio, PBC.

Sallan, L. C., & Coates, M. I. (2010). End-Devonian extinction and a bottleneck in the early evolution of modern jawed vertebrates. *Proceedings of the National Academy of Sciences*, *107*(22), 10131–10135. https://doi.org/10.1073/pnas.0914000107

Sallan, L. C., & Coates, M. I. (2013). Styracopterid (Actinopterygii) ontogeny and the multiple origins of post-Hangenberg deep-bodied fishes. *Zoological Journal of the Linnean Society*, *169*(1), 156–199. https://doi.org/10.1111/zoj.12054

Sallan, L. C., & Friedman, M. (2012). Heads or tails: staged diversification in vertebrate evolutionary radiations. *Proceedings of the Royal Society B: Biological Sciences*, *279*(1735), 2025–2032. https://doi.org/10.1098/rspb.2011.2454

Sallan, L. C., & Galimberti, A. K. (2015). Body-size reduction in vertebrates following the end-Devonian mass extinction. *Science*, *350*(6262), 812–815. https://doi.org/10.1126/science.aac7373

Schaeffer, B., & Rosen, D. E. (1961). Major Adaptive Levels in the Evolution of the Actinopterygian Feeding Mechanism. *American Zoologist*, *1*(2), 187–204. doi:10.1093/icb/1.2.187

Stensio, E. A. (1947). The sensory lines and dermal bones of the cheek in fishes and amphibians. *Kungliga Svenska Vetenskapsakademiens Handlingar*, *3*(24), 1–195.

Streelman, J. T., & Danley, P. D. (2003). The stages of vertebrate evolutionary radiation. *Trends in Ecology & Evolution*, *18*(3), 126–131. https://doi.org/10.1016/S0169-5347(02)00036-8

Tang, W., Pe-Piper, G., Piper, D. J. W., Chen, A., Hou, M., Guo, Z., & Zhang, Y. (2024). Architecture of lacustrine deposits in response to early Carboniferous rifting and Gondwanan glaciation, Nova Scotia, south-east Canada. *Sedimentology*, *71*(2), 457–485. https://doi.org/10.1111/sed.13140

Tibert, N. E., & Scott, D. B. (1999). Ostracodes and agglutinated foraminifera as indicators of paleoenvironmental change in an Early Carboniferous Brackish Bay, Atlantic Canada. *Palaios*, *14*(3), 246–260. https://doi.org/10.2307/3515437

Wainwright, P. C., & Bellwood, D. R. (2002). Ecomorphology of Feeding in Coral Reef Fishes. In P. F. Sale (Ed.), *Coral Reef Fishes* (pp. 33–55). Academic Press.

Wilson, C. D., Mansky, C. F., & Anderson, J. S. (2021). A platysomid occurrence from the Tournaisian of Nova Scotia. *Scientific Reports*, *11*(1), 8375. https://doi.org/10.1038/s41598-021-87027-y

Wilson, C. D., Pardo, J. D., & Anderson, J. S. (2018). A primitive actinopterygian braincase from the Tournaisian of Nova Scotia. *Royal Society Open Science*, *5*(5), 171727. https://doi.org/10.1098/rsos.171727

Handling Editor: Carole Burrow.